Nanoscale

Light beams with selective angular momentum generated by hybrid plasmonic waveguides

Journal:	*Nanoscale*
Manuscript ID:	NR-COM-06-2014-003606.R1
Article Type:	Communication
Date Submitted by the Author:	07-Aug-2014
Complete List of Authors:	Liang, Yao; South China Normal University, Huang, Xu Guang; South China Normal University, School for Information and Optoelectronic Science and Engineering Wu, Hanwen; South China Normal University, School for Information and Optoelectronic Science and Engineering Huang, Ginjie; National University of Singapore, Department of Electrical and Computing Engineering

Cite this: DOI: 10.1039/c0xx00000x

www.rsc.org/xxxxxx

Communication

Light beams with selective angular momentum generated by hybrid plasmonic waveguides

Yao Liang,[a] Han Wen Wu,[a] Bin Jie Huang,[b] and Xu Guang Huang*[a]

Received (in XXX, XXX) Xth XXXXXXXXX 20XX, Accepted Xth XXXXXXXXX 20XX

DOI: 10.1039/b000000x

We report an integrated compact technique that can "spin" and "twist" light on a silicon photonics platform, with the generated light beams possessing both spin angular momentum (SAM) and orbital angular momentum (OAM). It demonstrates the potential of SAM/OAM optics for on-chip integration.

Light beams can convey angular momentum (AM) through two different components: the intrinsic component–the spin angular momentum (SAM) associated with the handedness of circular or elliptical polarization, and the quasi-intrinsic component–the orbital angular momentum (OAM) associated with a spiral phase front.[1-2] Light beams possessing SAM or OAM have been extensively investigated recently for numerous applications, ranging from free-space optical communication,[3] imaging[4] to biological detection,[5] including quantum-information processing as an important example.[6] In particular, light beams carrying AM have unique applications in micro particles manipulation,[7] owing to the fact that AM can be transferred on the absorbing particle when light beams impinge on it.[8]

Various methods have been established to produce beams carrying SAM/OAM. Traditionally, the SAM beams are created by using quarter-wave plates.[9] The OAM beams are usually generated by shaping of the phase front of a laser as it passes through different optical devices, such as spiral phase plates,[10] cylindrical lens mode converter[11] and spatial light modulators.[12] A common disadvantage to all of those bulk optical devices is mechanical complexity since moving components, such as lenses, mirrors and phase plates, are required. In addition, their sizes are relatively large, ranging from tens of micron to several millimeters. As a result, those optical devices are not convenient for future complex research activities. In many applications, people would want to use compact, functional components in the form of photonic integrated circuits (PICs) fabricated on optical waveguides,[13-14] and may want to achieve complex functions using controllable AM with broadband operation. Innovations, however, to integrate SAM/OAM optics have been so far limited. One previous example is Chirally Coupled Core Fiber (CCCF) with a "side core" chirally winding around the center core following a helical path.[15] The structure is able to generate light beams carrying both of SAM and OAM. However, the CCCF is quite complex in structure and very large since its length is in millimetre scale, which is not suitable for the realization of PICs chip. Another interesting scheme is known as ultral-thin metasurfaces with space-variant array of plasmonic gold nano-antennas.[16-17] These devices are capable of spin-to-orbit coupling, which means, they can generate light carrying OAM from light initially carrying only SAM. The OAM beams generated in such devices work well in free space, but not in optical waveguides. The third innovative scheme to generate OAM beams is known as microring OAM emitter with angular grating.[18] Such structure is based on microring resonator with only a few microns in size. However, the microring resonator has frequency selectivity, which means only resonant frequencies are supported, resulting in a discrete frequencies operation. Another challenge of the design is that the OAM beams are emitted out into free space rather than propagate inside optical waveguides, thus it is not very practical for some applications, i.e. encoding quantum information on-chip.

In this work, we address these challenges by proposing, for the first time to our knowledge, a scheme that can generate light beams with selective AM over a broad wavelength range by using hybrid plasmonic waveguide,[19] as seen in Fig. 1. The generated AM beams can either propagate in optical waveguides or emit into free space. Furthermore, this approach is of favourable fabrication feasibility since it is based on silicon-on-insulator (SOI) platform using standard complementary metal oxide

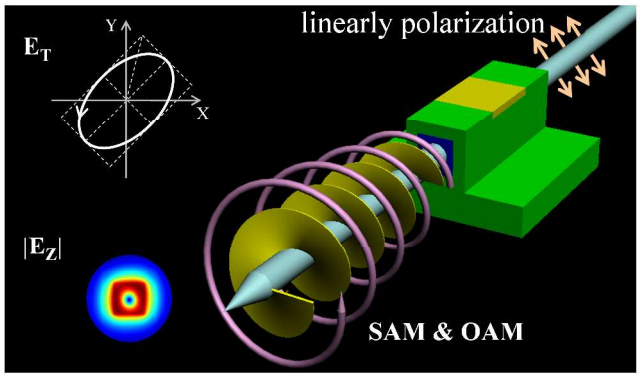

Fig. 1 The abridged general view of the generation process of AM light beam, with the dominant transverse electric field component E_T carrying SAM and the longitudinal component E_Z carrying OAM.

[a] *School of Information and Optoelectronic Science and Engineering, South China Normal University, Guangzhou 510006, China. Tel: +86 18928925528; E-mail: huangxg@scnu.edu.cn .*

[b] *Department of Electrical and Computing Engineering, National University of Singapore, Singapore 117583, Singapore.*

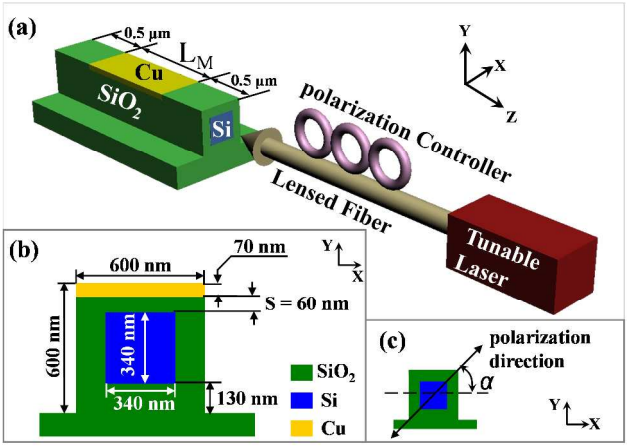

Fig. 2 (a) 3D schematics (not to scale) of the proposed scheme, and the coordinate system used. (b) Cross sectional view of the geometry of the hybrid plasmonic section. (c) The definition of the initial polarization direction angle α.

semiconductor (CMOS) technology.[20] Fig. 2(a) shows the schematic of the suggested method. The key part of the suggested method is an optical waveguide, consisting of three sections: the first and third sections are pure dielectric waveguides with a square silicon (Si) core surrounded by silica (SiO_2) cladding, and the middle section is a hybrid plasmonic waveguide. The generation of SAM and OAM happens in the hybrid section, where the copper (Cu) layer is located upper of the silicon nanowire with 60 nm silica spacer (S) between them, the geometry of which is shown in Fig. 2(b). A precision tunable laser is involved in the proposed scheme and its power is coupled into the first waveguide section by using a tapered fibre lens tip. When coupled into the first waveguide section through a tapered fibre lens tip, the light beam needs to propagate a certain distance to form a stable mode distribution. Thus, a 0.5 μm long first dielectric waveguide section is required. Similar situation happens when light travels from the second waveguide section to the third section, and thus a 0.5 μm long third dielectric waveguide section is also needed. A conventional or integrated polarization controller (PC)[21] is used to control the initial linearly polarization state of the light beam coupled into the optical waveguide, with the polarization direction angle written as α, as seen in Fig. 2(c).

A possible fabrication scheme for practical implementation is proposed as follows: (1) the Si waveguide is etched into a standard Si-on-insulator (SOI) wafer; (2) The process of thermal oxidation is followed, to form a SiO_2 thin film with a thickness of 130 nm at the top and sidewalls of Si core; (3) A photoresist film is deposited and patterned to create a narrow slot window at the top of the second waveguide section; (4) A focused ion beam (FIB) technique with nanoscale resolution is applied to etch unwanted SiO_2, in order to form a suitable groove prepared for copper deposition and to make sure a 60 nm SiO_2 spacer at the top of Si core; (5) After the deposition of Cu, a lift off is performed, resulting in a copper layer at the top of Si core.

Hybrid plasmonic waveguides can exhibit large birefringence.[22] Here we use this characteristic to make light beams "spin" and "twist". Providing that the initial linearly polarization direction is neither parallel to x-axis nor y-axis, the

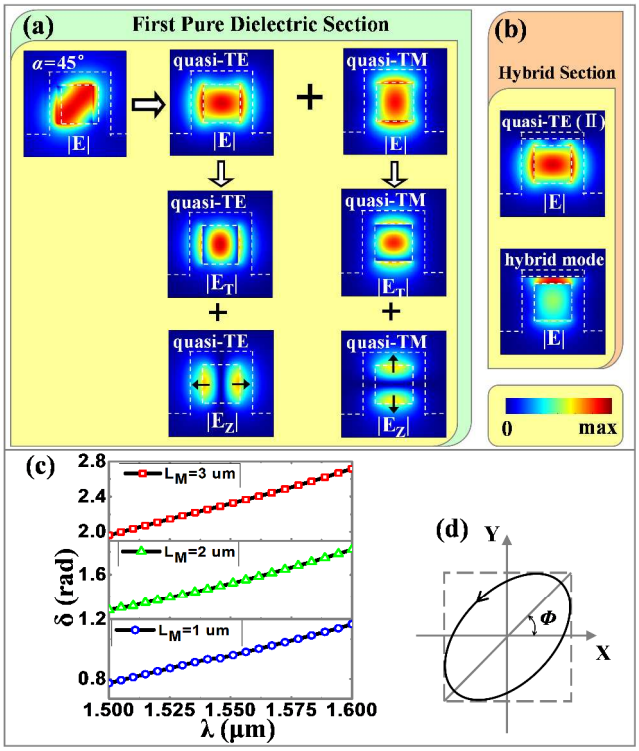

Fig. 3 (a) Amplitude distributions of a 45° polarized beam, and its decomposed components: a quasi-TE mode and a quasi-TM mode, in the first waveguide section. E_T and E_Z are the corresponding transversal and longitudinal components. The opposite directions of arrows, in $|E_Z|$ distributions, represent two different values, either positive or negative. The boundaries are shown by dashed lines. (b) Amplitude distributions of the quasi-TE (II) mode and the hybrid mode in the hybrid plasmonic section. (c) The wavelength dependence of relative phase δ for L_M = 1, 2, 3 μm. (d) The E_T polarization state of the output beam, charactered with the amplitude ratio (tan(Φ)) and the relative phase (δ) between E_Y and E_X.

α-angle polarized mode supported by the first pure dielectric waveguide section can be decomposed into two orthogonal components: a quasi-transverse magnetic (TM) mode with the dominant transverse electric field component (E_T) parallel to the y-axis (E_Y) and a quasi-transverse electric (TE) mode with E_T parallel to the x-axis (E_X),[23] as seen in Fig. 3(a). For a quasi-TM mode, it can mainly be decomposed into a dominant transverse component E_T and a longitudinal component E_Z, and so does a quasi-TE mode (Fig. 3(a)). Hence, the initial polarization direction angle α can be defined by: $\tan(\alpha) = (|E_{T\text{-}TM1}| / |E_{T\text{-}TE1}|)$, where $|E_{T\text{-}TM1}|$ and $|E_{T\text{-}TE1}|$ are the E_T amplitudes of the quasi-TM and -TE modes in the first waveguide section.

The low 0^{th}-order modes, the quasi-TE and -TM modes, will only be discussed, because higher order modes of interest are restrained in the proposed waveguide at the wavelength of 1.55 μm. Mode profile distributions can be investigated by using the eigenmode expansion method. In the first pure dielectric waveguide section, the effective index is 2.314 for the quasi-TE mode, and 2.321 for the quasi-TM mode. In this case, the effective index difference (Δn) between these two modes is so small (0.007) that it can almost be negligible. However, this difference will be remarkably enlarged when light beams travel in the hybrid plasmonic waveguide section. In the hybrid plasmonic

waveguide section, the quasi-TE mode is coupled into another asymmetric quasi-TE mode (quasi-TE(□)) while the quasi-TM mode is converted into a hybrid plasmonic mode (Fig. 3(b)), and their effective indices are 2.256 + 0.0025i and 2.440 + 0.0029i, respectively. In this case, only the real parts are of interest since they can affect the phase shift, and their difference is 0.184, which is about two orders of magnitude bigger than the previous one. Therefore, after passing through the hybrid section, light will be coupled into the quasi-TE and -TM modes again but with a relative phase (δ) between them. The relative phase δ is preserved by the birefringence of hybrid plasmonic waveguide as well as other factors such as the modes coupling processes among different waveguide sections. The existence of relative phase δ between the two orthogonal components suggests that light beams do "spin" in the third waveguide section, which means the SAM is generated. This relative phase δ between these two components will not only result in "spinning" but also "twisting" of light beams, which we will prove it later. The relative phase δ can be written as:

$$\delta = k_0 \Delta n L_M + \Delta\delta \quad (1)$$

where k_0 is free space wave number, Δn the effective index difference in hybrid plasmonic section, L_M the length of metal (Cu), and Δδ the phase difference caused by other factors. The requirement of the phase delay of π/2 results in $L_M \approx 2.11\mu m$, assuming that Δn = 0.184, λ= 1.55 μm, and Δδ = 0.

A three dimensional finite difference time domain (3D-FDTD) method is used to confirm our previous analysis. Initially, we set the initial linearly polarization direction angle to be α = 45°. An increase in the length of Cu (from 1μm to 2μm, 3μm) leads to an increase in the relative phase δ over a broad wavelength range, the result of which is shown in Fig. 3(c). Moreover, the relative phase δ shows a linear dependence on the wavelength (λ): the longer the wavelength is, the larger the relative phase will be. Hence, one can set arbitrary value of relative phase δ by tuning of the metal length L_M. The simulated relative phase δ is around π/2 at λ = 1.55 μm when the metal length is set as L_M = 2 μm, which is in agreement with the calculted result of L_M from Eq. (1).

The polarization state of the polarized light is charactered with the amplitude ratio (tan(Φ)) and the relative phase (δ) between E_Y and E_X (the E_T components of the quasi-TM and -TE modes), as seen in Fig. 3(d). The parameter tan(Φ) is defined by: tan(Φ) = ($|E_{T\text{-}TM3}|$ / $|E_{T\text{-}TE3}|$), where $|E_{T\text{-}TM3}|$ and $|E_{T\text{-}TE3}|$ are the E_T amplitudes of the quasi-TM and -TE modes in the third waveguide section. The relationship between tan(Φ) and the initial polarization direction angle α can be expressed as:

$$\tan\Phi = \frac{|E_{T-TM3}|}{|E_{T-TE3}|} = \frac{k_1}{k_2}\frac{|E_{T-TM1}|}{|E_{T-TE1}|} = \frac{k_1}{k_2}\tan\alpha \quad (2)$$

where $0 < k_1, k_2 < 1$ are two constants related to the losses of the quasi-TM and -TE modes as light beams travel from the first waveguide section to the third waveguide section. Hence, one can set arbitrary value of tan(Φ) by tuning of the initial polarization direction angle α. For example, when changing α from 30° to 45° and 60°, the corresponding values of tan(Φ) are about 0.68, 1.04 and 1.58, respectively. It is worth noting that the ± signs of the initial polarization direction angle α determine the elliptical polarization state of the dominant transverse field component E_T (in the xy-plane) in the third waveguide section. For α > 0, with the polarization direction going through the first and the third quadrant of the xy-plane (Fig. 1(c)), there will be a left-handed (anticlockwise, defined from the point of view of the receiver) elliptical polarization state. For α < 0, with the polarization direction going through the second and the fourth quadrant of the xy-plane, there will be a right-handed elliptical polarization state. For a single photon, the SAM can have two discrete values of $\pm\hbar$, with $-\hbar$ for right-handed and $\hbar$ for left-handed circular polarizations.[24]

However, the output light beams in the third waveguide section are not so called conventional elliptical polarization light, because the longitudinal electric field component (E_Z) is not identically zero. As we will prove it later, the E_Z component is carrying OAM with a spiral phase wavefront.

Despite the fact that the polarization of an electromagnetic plane wave is purely transversal, a longitudinal electric field component E_Z can be found in a field with finite beam width.[25] Originally, the longitudinal electric field component E_Z is generated by the spatial derivative of the transverse components (E_X, E_Y),[26] thereby a large E_Z component can be generated by means of strong optical confinement.[23] In the homogeneous media such as the Si waveguide, the relationship between the complex amplitudes of transverse electric field E_T and E_Z is given by:[23]

$$E_Z = \frac{1}{i\beta}\nabla_T \cdot E_T \quad (3)$$

where β is the propagation constant and ∇_T is the transverse gradient. For quasi-TE and -TM modes, $\nabla_T \cdot E_T \approx \partial E_X / \partial x$ and

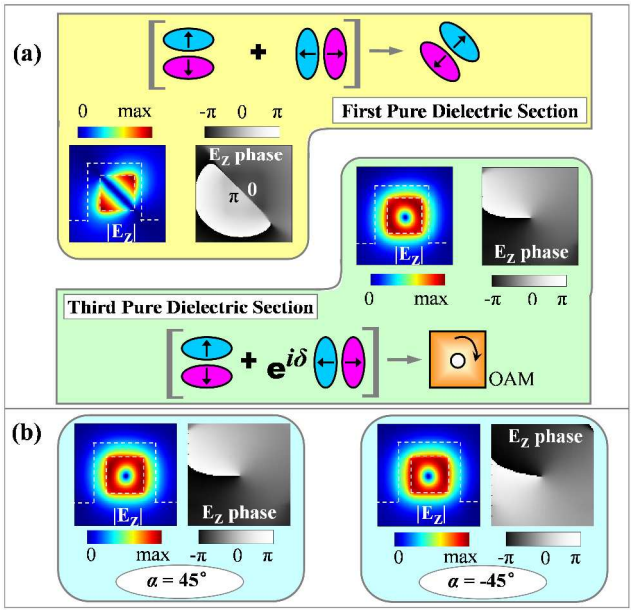

Fig. 4 (a) The superposition of the z-components of the quasi-TE and -TM modes in the first waveguide section. The abridged general view of the generation of OAM in the third waveguide section (the two z-components with a relative phase δ), and their corresponding field and phase distributions. (b) Simulated field and phase distributions of E_z in the third waveguide section for α = 45° and α = -45°. The operating wavelength λ = 1.55 μm and the metal length L_M = 2 μm. The boundaries are shown by dashed lines.

$\nabla_T \cdot E_T \approx \partial E_Y / \partial y$, respectively. By proper choosing the geometric parameters of Si waveguide, the amplitude of E_Z component can be as high as 97% of that of the dominant transverse electric field component E_T.[23] In our scheme, the amplitude of E_Z are around 78% of those of E_T for both the quasi-TE and -TM modes in the first and third waveguide sections, seen in Fig. 3(a).

As mentioned above, there is a relative phase δ between E_T components of the quasi-TE and -TM modes, mainly due to the birefringence of the hybrid plasmonic waveguide section. Examination of Eq. (3) reveals that the complex amplitude of E_Z is purely imaginary (by convention the transverse field is purely real), which means there is a fixed phase difference (π/2) between the E_T component and the E_Z component. As a result, the same relative phase δ does exist in E_Z components of the quasi-TE and -TM modes. Fig. 4(a) shows that the behavior of the E_Z components differ from each other in the first and third waveguide sections. In the first waveguide section, the quasi-TE mode is in phase with the quasi-TM mode, consequently, the superposition of their E_Z components results in an antisymmetric electric field distribution, with a discrete π phase shift distribution. In the third waveguide section, there is a relative phase δ between the quasi-TE and -TM modes, the consequence of the birefringence of the middle hybrid section. In this case, on the other hand, the superposition of E_Z components of the quasi-TM mode and the quasi-TE mode (with a relative phase δ that can be expressed as $e^{i\delta}$) results in an optical vortex possessing OAM, with a spiral phase distribution. Fig. 4(b) shows the field and the phase distributions of E_Z for α = 45° and α = -45°, with the operating wavelength λ = 1.55 μm and the metal length L_M = 2 μm. The z component of the electric field in the third waveguide section can be written as:

$$E_Z(r,\theta) = A(r)e^{im\theta} \quad (4)$$

where A(r) is the amplitude of the complex electric field, r and θ are the polar coordinates in the xy-plane, and m is an integer known as the topological charge of optical field. In this case, m = 1 for α = 45° and m = -1 for α = -45°, with the ± signs of m

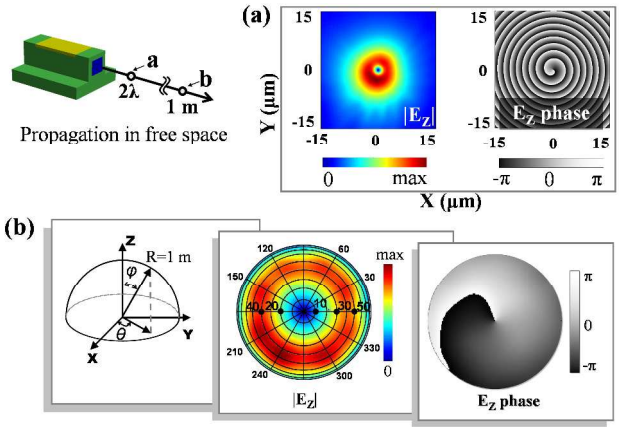

Fig. 5 The optical performance of the generated beam when it travels in free space. (a) The near field behavior: the electric field and phase distributions of E_z in the plane (parallel to xy-plane) 2λ (3.1μm) away from the output port. (b) The far field behavior: the electric field and phase distributions of E_z on the surface of a hemisphere that one meter away from the output port. The operating wavelength λ = 1.55 μm and the metal length L_M = 2 μm.

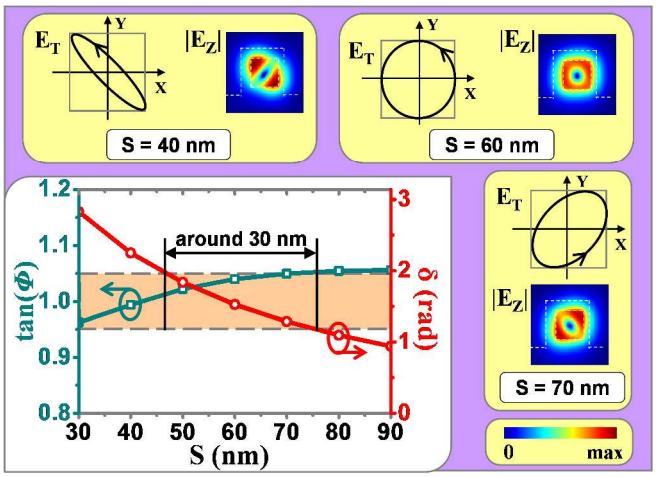

Fig. 6 Plots showing tan(Φ) and δ for the output beam as functions of the spacer thickness S, and drawings showing the elliptical polarization states of E_T and field distributions of the corresponding OAM component E_z, for different values of S, with (L_M, λ, α) = (2 μm, 1.55 μm, 45°).

depending on the handedness of the twist. Therefore, the ± signs of the initial polarization direction angle α determine not only the handedness of elliptical polarization state of the dominant transverse field component E_T but also the handedness of the optical vortex of the longitudinal component E_Z.

The light beam generated in our proposed scheme is tightly confined in the optical waveguide. There is no doubt that this "spin" and "twist" mode can travel inside the optical waveguide, steadily. However, when it emits out in free space, this tightly confined light beam diverges strongly. Fig. 5(a) shows that in free space, the longitudinal OAM component E_Z maintains its doughnut-like profile after 2λ (3.1μm) propagation distance away from the output port. Additionally, its phase distribution further confirms that the central null field (zero intensity) results from the phase singularity. To show the far field behavior of the generated beam in the proposed scheme, we plot the respective electric field and phase profiles of E_Z on the surface of a hemisphere that one meter away from the output port, as seen in Fig. 5(b). From this figure, one can clearly see that the longitudinal OAM component E_Z does not vanish after a long range propagation, with a dark hole (zero intensity) in the center. Its phase distribution, a spiral phase profile, further reveals that light is partially twisted like a corkscrew around its axis upon propagation. In the optical waveguide, the overall amplitude ratio between the longitudinal OAM component E_Z and the transverse SAM component E_T of the generated light beam is around 78%. In free space, on the other hand, the FDTD simulation results show that in the receive planes or surfaces, the ratio remains a constant for whatever propagation distance, such as λ/10, λ, 2λ and 1m.

Since the generated angular momentum is very much relied on the birefringence of the hybrid section, the geometric parameters in this section are expected to affect the angular momentum of the output beam. One important parameter is the thickness of the SiO_2 spacer (S) between the Si core and Cu layer (Fig. 2(b)). To illustrate this, we have considered the scenario when S changes from 30 nm to 90 nm, with (L_M, λ, α) = (2 μm, 1.55 μm, 45°). As shown in Fig. 6, the E_T polarized state of the output beam,

charactered with the amplitude ratio (tan(Φ)) and the relative phase (δ) between E_Y and E_X, is a function of S. In the proposed structure, the SAM and the OAM of output beam are inevitably related, which means, the polarization state of E_T will affect the field distribution of the OAM component E_Z. This characteristic is of great interest in optical manipulation, since different field distributions of E_Z might lead to different behaviors of nanoscale particles when this kind of light beam impinges on them. One might want a uniform and symmetrical field distribution of E_Z and a circular E_T. In this case, tan(Φ) should be set as 1 ± 5% and δ as $\pi/2 \pm \pi/8$, and thus the fabrication tolerance of the spacer thickness is about 30 nm, as seen in Fig. 6. Another important parameter is the metal length of the section hybrid section (Fig. 2(a)). The influence of the metal length on the output beam performance could be examined by Eq. (1). Giving the requirement of $\delta = \pi/2 \pm \pi/8$, the fabrication tolerance of L_M is calculated to be about 1μm near the point of L_M = 2 μm, with (S, λ, α) = (60 nm, 1.55 μm, 45°).

The generated light beam, with E_T carrying SAM and E_Z possessing OAM, is somehow similar to the tightly focused circularly polarized vortex beams in free space, which is generated by passing a circularly polarized light through a high numerical aperture (NA) lens, since the spin-to-orbital angular momentum transfer can occur in a strongly focused system.[27] In this case, however, complex bulk optical devices such as lenses and quarter-wave (λ/4) plates are required. In our study, such bulk optical devices are replaced with a compact hybrid plasmonic waveguide, the overall length of which is only 3 μm. Furthermore, the SAM and OAM carry quantum bit of information, and one can change the quantum states of SAM and OAM by simply changing the initial polarization direction angle, which suggests that our proposed scheme may be used in on-chip quantum information processing.

Conclusions

We have presented and numerically demonstrated a scheme that can generate light beams with selective SAM and OAM over a broad wavelength range. This is achieved by mainly introducing the strong optical mode confinement of a Si waveguide and the large birefringence of a hybrid plasmonic waveguide. The proposed scheme may form the basis for novel integrated SAM/OAM devices, and can be used to encode multiple bits of information onto a single photon through the effective usage of both SAM and OAM. Our work have demonstrated the potential of SAM/OAM optics for integration with the standard CMOS technology, and it will extend the applications of hybrid plasmonic waveguides and therefore unlock the full potentials of many interesting applications, ranging from increasing the channel capacity to providing secure communication in both classical and quantum regimes.

Acknowledgements

This work was supported by Project of Discipline and Specialty Constructions of Colleges and Universities in Education Department of Guangdong Province (2013CXZDA012), Program for Changjiang Scholars and Innovative Research Team in University (No. IRT13064), and Science and Technology Project of Education Department of Guangdong Province (2012KJCX0038).

Notes and references

1 L. Marrucci, E. Karimi, S. Slussarenko, B. Piccirillo, E. Santamato, E. Nagali, and F. Sciarrino, J. Optics-UK, 2011, **13**,064001.
2 S. Franke-Arnold, L. Allen, and M. Padgett, Laser Photonics Rev., 2008, **2**, 299-313.
3 J. Wang, J. Y. Yang, I. M. Fazal, N. Ahmed,Y. Yan, H. Huang, Y. Ren, Y. Yue, S. Dolinar, M. Tur, and A. E. Willner, Nat. Photonics, 2012, **6**, 488-496.
4 B. Jack, J. Leach, J. Romero, S. Franke-Arnold, M. R. Marte, S. M. Barnett, and M. J. Padgett, Phys. Rev. Lett., 2009, **103**, 083602-083605.
5 S. Zhang, J. Zhou, Y. Park, J. Rho, R. Singh, S. Nam, A. K. Azad, H. T. Chen, X. Yin, A. J. Taylor, and X. Zhang, Nat. Commun., 2012, **3**, 942-948.
6 R. Fickler, R. Lapkiewicz, W. N. Plick, M. Krenn, C. Schaeff, S. Ramelow, and A. Zeilinger, Science, 2012, **338**, 640-643.
7 W. Y. Tsai, J. S. Huang , and C. B. Huang, Nano Lett., 2014, **14** , 547-552.
8 M. Woerdemann, C. Alpmann, M. Esseling and C. Denz, Laser Photonics Rev., 2013, **7**, 839-854.
9 A. Pors, and S. I. Bozhevolnyi, Opt. Express, 2013, **21**, 2942-2952.
10 M. W. Beijersbergen, R. P. C. Coerwinkel, M. Kristensenl, and J. P. Woerdman, Opt. Commun., 1994, **112**, 321-327.
11 J. Courtial, and M. J. Padgett, Opt. Commun., 1999, **159**,13-18.
12 N. R. Heckenberg, R. McDuff, C. P. Smith, and A. G. White, Opt. Lett., 1992, **17**, 221-223.
13 J. Tao, Q. J. Wang, B. Hu, and Y. Zhang, Nanotechnology, 2012, **23**, 444014.
14 M. Cohen, Z. Zalevsky and R. Shavit, *Nanoscale*, 2013, **5**, 5442-5449.
15 X. Ma, C. H. Liu, G. Chang, and A. Galvanauskas, Opt. Express, 2011, **19**, 26515-26528.
16 P. Genevet,N. Yu, F. Aieta, J. Lin, M. A. Kats, R. Blanchard, M. O. Scully, Z. Gaburro,and F. Capasso, Appl. Phys. Lett., 2012, **100**, 013101.
17 E. Karimi, S. A Schulz, I. D. Leon, H. Qassim, J. Upham, and R. W Boyd, Light-Science & Applications, 2014, **3**, e167.
18 X. Cai, J. Wang, M. J. Strain, B. J. Morris, J. Zhu, M. Sorel, J. L. O'Brien, M. G. Thompson, and S. Yu, Science, 2012, **338**, 363-366.
19 R. F. Oulton, V. J. Sorger, D. A. Genov, D. F. P. Pile, and X. Zhang, Nat. Photonics, 2008, **2**, 496-500.
20 S. H. Jo, W. Lu, Nano Lett., 2008, **8**, 392-397.
21 L. Jin, Q. Chen, and L. Wen, Opt. Lett., 2014, **39**,2798-2801.
22 M. Z. Alam, J. N. Caspers, J. S. Aitchison, and M. Mojahedi, Opt. Express, 2013, **21**, 16029-16034.
23 J. B. Driscoll, X. Liu, S. Yasseri, I. Hsieh, J. I. Dadap, and R. Osgood, Jr, Opt. Express, 2009, **17**, 2797-2804.
24 R. A. Beth, Phys. Rev., 1936, **50**,115.
25 B. Richards, and E. Wolf, Proc. R. Soc. A, 1959, **253**, 358-379.
26 A. Boivin, and E. Wolf, Phys. Rev., 1965, **138**, B1561-B1565.
27 Y. Zhao, J. S. Edgar, G. D.M. Jeffries, D. McGloin, and D. T. Chiu, Phys. rev. lett., 2007, **99**:073901.